

PAPER • OPEN ACCESS

Methodologies for model parameterization of virtual CTs for measurement uncertainty estimation

To cite this article: Felix Binder *et al* 2022 *Meas. Sci. Technol.* **33** 104002

View the [article online](#) for updates and enhancements.

You may also like

- [Internal surface roughness measurement of metal additively manufactured samples via x-ray CT: the influence of surrounding material thickness](#)
Joseph John Lifton, Yuchan Liu, Zheng Jie Tan *et al.*
- [Electron-optical in-situ metrology for electron beam powder bed fusion: calibration and validation](#)
Christopher Arnold and Carolin Körner
- [3D Printed Flow Field and Fixture for Visualization of Water Distribution in Fuel Cells by X-ray Computed Tomography](#)
Robin T. White, Francesco P. Orfino, Mohamed El Hannach *et al.*

Methodologies for model parameterization of virtual CTs for measurement uncertainty estimation

Felix Binder^{1,*} , Benjamin A Bircher² , René Laquai³, Alain Küng², Carsten Bellon⁴ , Felix Meli² , Andreas Deresch⁵, Ulrich Neuschaefer-Rube³  and Tino Hausotte¹ 

¹ Institute of Manufacturing Metrology (FMT), Friedrich-Alexander University Erlangen-Nuremberg (FAU), Erlangen, Germany

² Federal Institute of Metrology (METAS), Laboratory for Length, Nano- and Microtechnology, Bern-Wabern, Switzerland

³ Physikalisch-Technische Bundesanstalt (PTB), Braunschweig, Germany

⁴ Bundesanstalt für Materialforschung und -prüfung (BAM), Berlin, Germany

⁵ YXLON International GmbH, Hamburg, Germany

E-mail: felix.binder@fmt.fau.de

Received 29 January 2022, revised 31 May 2022

Accepted for publication 22 June 2022

Published 8 July 2022



Abstract

X-ray computed tomography (XCT) is a fast-growing technology for dimensional measurements in industrial applications. However, traceable and efficient methods to determine measurement uncertainties are not available. Guidelines like the VDI/VDE 2630 Part 2.1 suggest at least 20 repetitions of a specific measurement task, which is not feasible for industrial standards. Simulation-based approaches to determine task specific measurement uncertainties are promising, but require closely adjusted model parameters and an integration of error sources like geometrical deviations during a measurement. Unfortunately, the development of an automated process to parameterize and integrate geometrical deviations into XCT models is still an open issue. In this work, the whole processing chain of dimensional XCT measurements is taken into account with focus on the issues and requirements to determine suitable parameters of geometrical deviations. Starting off with baseline simulations of different XCT systems, two approaches are investigated to determine and integrate geometrical deviations of reference measurements. The first approach tries to iteratively estimate geometric deviation parameter values to match the characteristics of the missing error sources. The second approach estimates those values based on radiographs of a known calibrated reference object. In contrast to prior work both approaches only use a condensed set of parameters to map geometric deviations. In case of the iterative approach, some major issues regarding unhandled directional dependencies have been identified and discussed. Whereas the radiographic method resulted in task specific expanded measurements uncertainties below one micrometre even for bi-directional features, which is a step closer towards a true digital twin for uncertainty estimations in dimensional XCT.

* Author to whom any correspondence should be addressed.



Original content from this work may be used under the terms of the [Creative Commons Attribution 4.0 licence](https://creativecommons.org/licenses/by/4.0/). Any further distribution of this work must maintain attribution to the author(s) and the title of the work, journal citation and DOI.

Keywords: x-ray computed tomography, virtual CT, uncertainty estimation, geometrical deviation, parameterization

(Some figures may appear in colour only in the online journal)

1. Introduction

Estimating the uncertainty of an x-ray computed tomography (XCT) measurement is challenging. Following the guideline of VDI/VDE 2630 Part 2.1 [1] at least 20 repetitions of the measurement have to be conducted to estimate the measurement uncertainty of a given task. Alternatively, a simulation-based approach like the uncertainty estimation according to the guide to the expression of uncertainty in measurement (GUM) supplement 1 [2] requires a representative model of the XCT system. In recent years, several XCT simulation software packages have been developed which use analytical and statistical methods to generate projection images close to actual XCT measurements. However, if the simulations are based on ideal geometries usually a disparity between simulation and measurement has to be accepted. In the previous European metrology programme for innovation and research (EMPIR) project Microparts (IND59) [3] it was shown, that the gap between an adapted simulated model and an actual measurement can be reduced considerably, if geometrical deviations are incorporated. However, the estimation of those geometrical deviations required expert knowledge according to [4], which is not feasible for industrial standards. Therefore, in the EMPIR project AdvanCT (17IND18) [5] a systematic procedure has been explored, to include geometrical deviations in virtual XCT models.

In the following chapter, first a short overview of ongoing research towards XCT simulations will be given. Afterwards, in section 3 a general methodology to determine virtual XCT parameters is provided. For that purpose, a framework is used to compare simulated and measured volumes. After that, two experimental methods are presented to determine geometrical deviation parameters either by an iterative adaption routine or by radiographic reference measurements. In section 4 different test scenarios are assessed, to verify if the resulting geometrical deviation parameters are plausible and can be transferred to other XCT systems. Finally, limitations and experiences of the experimental work are discussed in section 5.

2. State of the art

There are several radiographic simulation tools available, like aRTist [6, 7], Scorpius XLab [8], SimCT [9] or CIVA CT [10] to simulate XCT measurements. Reiter and Kastner [11] used SimCT to study different uncertainty errors in computed tomography with an aluminium workpiece that has three defined diameters of interest. Helmecke *et al* [4] focused on a comparison between an adapted aRTist simulation and the VDI/VDE 2630 Part 2.1 method with an aluminium rotor. Hiller and Reindl [12] used Scorpius XLab and a hollow aluminium cylinder to evaluate simulated deviations in different scenarios.

Those previous studies used different approaches, workpieces, XCT systems and even simulation software, but showed in their specific case, that a simulation model with adjusted parameters can be close to a given XCT system reference.

Even though those case studies demonstrated the potential of XCT simulations, a general and traceable model of arbitrary XCT systems is currently not available. Therefore, several research projects were granted to further improve partial aspects towards a virtual XCT. For example, the EMPIR funded project NanoXSpot (18NRM07) is researching on a traceable measurement method for focal spot sizes below 5 μm , which has an essential contribution to the projection image unsharpness [13]. Another example is the research project CTSimu (WIPANO, 03TNH026A), which is working on a basic qualification guideline of XCT simulation software in preparation for the VDI/VDE 2630 Part 2.2 [14]. Those grants show that the characterization and virtualization of XCT systems are important topics, but to induce substantial impact for industry and society a global and systematic procedure to obtain a complete digital twin model is required.

However, such a systematic procedure has to consider all major error sources of an actual XCT system. In a prior study [15] geometrical deviations—which are well known to be a major error source in XCT—have been approached to integrate in a virtual CT model. Albeit, this integration required manual user inputs and is based on an elaborated guess of the parameter range. To further address those issues, two approaches have been investigated to integrate geometrical deviations systematically into a given CT simulation.

3. Methodology

In this chapter, a general methodology to determine virtual XCT parameters is proposed, which focusses on establishing similar conditions between XCT measurements and simulations. Therefore, an already established conceptual framework is provided in section 3.1, which takes the complete process for a dimensional XCT measurement into account and demonstrates an actual implementation.

XCT simulations are usually based on an ideal computer-aided design (CAD) geometry, whereas the derived geometry by XCT measurements depends on the manufactured sample. In section 3.2 the cumulated surface deviation of an actual to nominal comparison between the resulting volumes and a corrected CAD model is introduced as a considered parameter to compare simulated and measured volumes.

Section 3.3 focusses on geometrical deviations, which can cause an underestimation of dimensional features if not considered in the virtual model of an XCT simulation. The estimation of 21 geometrical parameters for a specific CT is a complex issue. However, a Pareto analysis showed, that a reduced

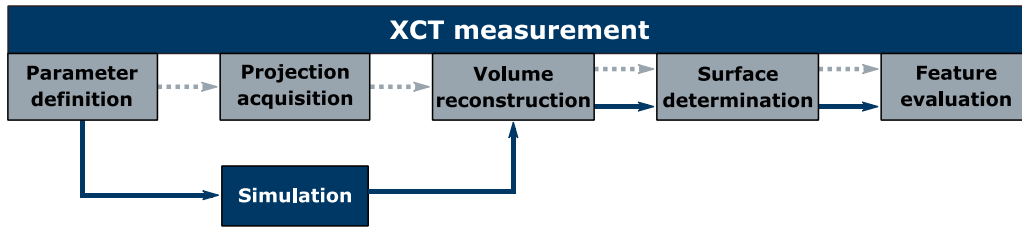


Figure 1. Integration of XCT simulations in the dimensional XCT measurement process.

Table 1. XCT system settings for the repeated measurement series of the hole plate reference.

Assembly:		Source:		Detector:	
SOD:	275.13 mm	Voltage:	170 kV	Size:	(409.6 × 409.6) mm
SDD:	1376.78 mm	Current:	250 μA	Pixel:	(2048 × 2048) px
Orientation:	30° tilted	Pre-filter:	Cu, 0.25 mm	Integration time:	2000 ms
Magnification:	5.00	Spot size:	43 μm	Gain:	8×
				Binning:	1 × 1
				Averaging:	None

SDD: Source to detector distance

SDD: Source to detector distance

set of six parameters is sufficient to cover the dominant influences of the geometrical deviations.

Based on that assumption, two experimental approaches either estimate the unknown geometrical deviations with parameter optimization (see section 3.4.1) or by assessing their values determined from radiographs of a calibrated multi-sphere standard (see section 3.4.2).

3.1. Framework

A general framework that can be applied to most industrial XCT systems must be applicable to a variety of established processing methods, different hardware setups and specific measurement strategies. Therefore, a suitable framework for this task is based on the general concept to keep the simulation as close as possible to the actual XCT measurement [4, 12]. This includes a simulation model, whose parameters are closely adapted to the behaviour of the XCT system. It also includes the usage of the same applications and settings for processing steps like the reconstruction, the surface determination and the feature evaluation. In this way, differences which are caused by different implementations are expected to be reduced. The used framework is summarized in figure 1.

For an actual implementation of the framework, a suitable XCT measurement is required as a template. The template should represent a standard measurement within the operating range of the XCT system to reduce artefacts. As reference, a (48 × 48 × 8) mm³ aluminium plate (PTB_A14) with 28 holes (∅ 4.0 mm) placed along seven different directions has been used and evaluated according to [16]. The hole plate was repeatedly measured 20 times with a Zeiss Metrotom 1500 and the settings from table 1 to create a suitable reference sample. For the setup of the virtual XCT model, the radiographic simulation aRTist [17] (v. 2.10.1) has been used.

aRTist combines analytical and Monte-Carlo based methods to simulate the radiation transport of a customizable XCT

setup. A typical cone beam scan with a circular trajectory can be simulated with the integrated *CtScan* module. For a basic simulation setup several parameter inputs are necessary which have been summarized in figure 2.

Most of the parameters can be derived as nominal values directly from the settings of the reference measurement (compare table 1). However, the source and the detector model setups need a further detailed adjustment to resemble the measurement reference. In case of the investigated Zeiss Metrotom system, the source spectrum has been generated with the aRTist spectrum generator [19]. Necessary settings, like the target thickness, the angle of electron incidence and the window material and thickness have been provided as nominal values by the manufacturer. The focal spot size S_F was estimated by the source power P_S with $S_F \approx P_S \frac{\mu\text{m}}{\text{W}}$ for $P_S \geq 7\text{W}$, which is based on the provided values of the operating software Metrotom OS. The focal spot is weighted with a 2D Gaussian function with a full width at half maximum (FWHM) of 18.6 μm and was determined based on the derivatives of the unsharpness contributions along a sharp edge profile according to Orgeldinger *et al* [20]. Alternatively, a standard test method for measurements of focal spots and industrial x-ray tubes by pinhole imaging exists and is described in the ASTM E1165 [21].

The detector can be modelled in aRTist in three different ways. If the size and material composition of the active detector layers are known, the sensitivity of the detector can be estimated with the *DetectorCalc* module. A standardized way to set up a detector model is provided with the *DigRad* module, which generates a detector model based on characteristic values determined according to the ASTM E 2597 [22]. In case of the investigated system, an experimental detector model has been generated based on a series of repeated half image projections at the tube settings of table 1. The mean grey values and the signal to noise ratios according to EN ISO 15708-3 [23] were extracted from those projections. The corresponding

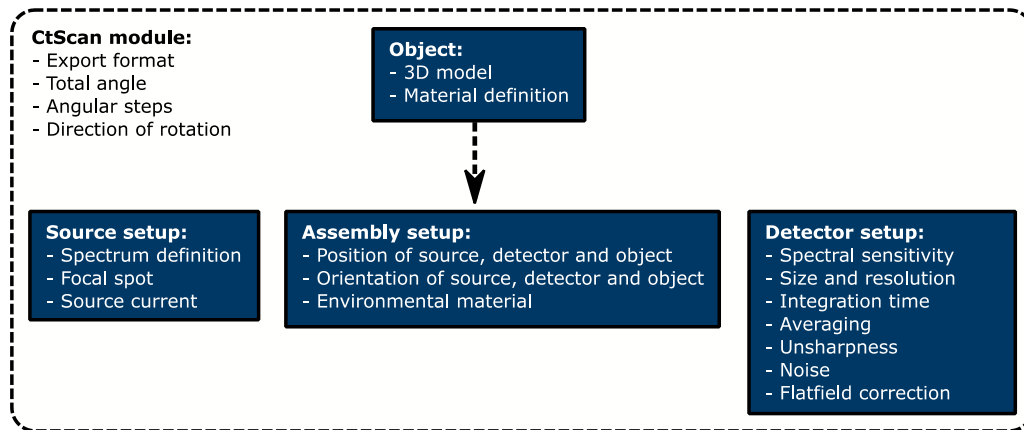


Figure 2. Overview of the necessary parameters to run the *CtScan* module in aRTist [18].

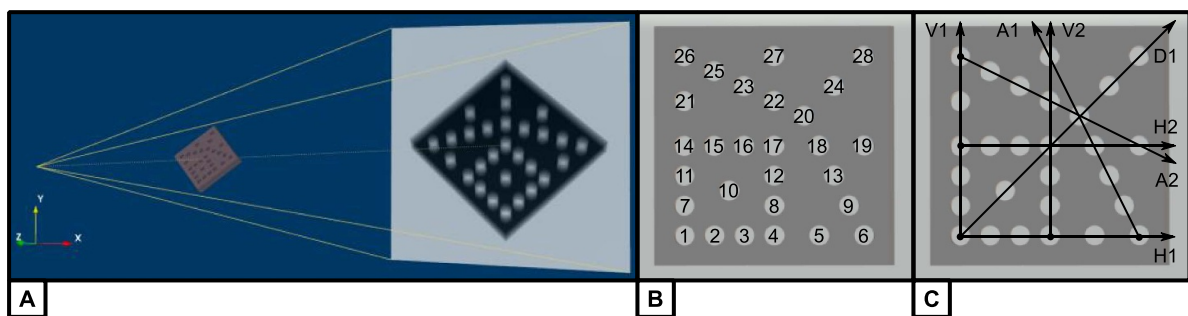


Figure 3. Display of a rendered projection of the hole plate setup in aRTist (A) with hole identifiers (B) and directional groups (C).

energy densities, which are needed to fully describe the characteristic and noise curve, were calculated according to the proposed method of Wohlgemuth *et al* [24]. The detector unsharpness was estimated to be 0.6 mm, which also resulted from the previously described edge profile study. To compensate the cone beam characteristic, the aRTist internal option to perform a flat-field correction was enabled.

Following the suggested framework in figure 1, aRTist will only be used to simulate projection images, even though it provides an option to use an integrated Feldkamp–Davis–Kress (FDK) reconstruction for further processing. Therefore, the common interface between an actual measurement and the simulation is chosen to be a stack of flat field corrected projections. From here on, the measured and the simulated data is reconstructed and analysed with the same settings and the same evaluation software VG Studio MAX (v.3.5). An overview of the hole plate placement inside the simulation setup is provided in figure 3, which concludes the implementation of the proposed framework in aRTist.

3.2. Comparison parameters

Comparing simulated data to actual measurements is challenging, due to several disparities. For example, the measured data is derived from an actual manufactured workpiece, whereas the simulated object is usually provided by an ideal CAD geometry or a triangulated surface mesh (TSM). Any deviations between these two objects, will automatically introduce systematic errors, which propagate themselves with

any additional processing step. Using selected features as suitable comparison criteria like uni- or bi-directional distances are often biased by the chosen measurement strategy. To avoid those influences, the surface deviations compared to a common ground truth have been chosen as a robust comparison criterion. For the required ground truth, three options have been considered:

- The whole nominal geometry of the measured workpiece.
- An extracted surface mesh from a previous XCT measurement of the workpiece.
- A partial area of a surface mesh corrected with coordinate measuring machine (CMM) reference measurements.

If the whole nominal geometry is used as a ground truth to compare the resulting deviations from simulated and measured surfaces, any imperfection of the manufactured workpiece will be part of the deviation distribution. This results in a biased parameter estimation.

Using the extracted surface of a previously determined XCT volume reduces the differences between the simulation and the measurement and therefore will increase similarity. However, a highly detailed extracted surface mesh increases the necessary computational time for each simulation due to the additional vertices. Consequently, the details of the mesh would have to be reduced, which has a filtering effect and introduces another bias.

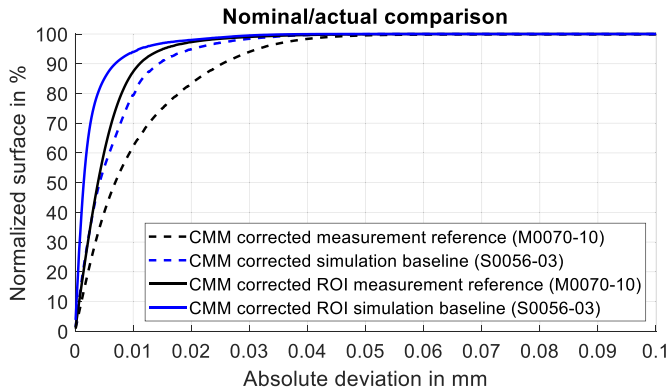


Figure 4. Exemplary nominal/actual comparison of a measurement reference and the simulation baseline considering either the whole surface of a CMM corrected CAD as ground truth or only the inner hole areas as region of interest.

The third option combines the first two approaches, but requires an additional reference system. To reduce the influence of workpiece deviations due to the manufacturing process, not the whole surface is considered as ground truth. Instead, only the relevant regions of interest (ROIs), which later are evaluated to measure dimensional features, are considered. Therefore, not the whole workpiece has to be manufactured accurately, but only partially in the defined ROIs, which reduces the distance between the cumulated deviation graphs of the simulation and measurement as seen in figure 4. To further increase the similarity of the chosen ROI areas, the centre positions and the diameters of the drilled holes have been adjusted in the nominal CAD model according to a CMM reference measurement. In case of the hole plate workpiece this resulted only in a small improvement, since the holes were already manufactured with high precision.

The remaining systematic offset between the surface deviations of the hole ROIs of the baseline simulation and the measured workpiece indicates, that the measurement reference is influenced by more deviation sources than the simulation currently reflects.

3.3. Geometrical deviations

Geometrical deviations during an XCT scan can be caused for example by temperature gradients, vibrations or inaccuracies of the positioning system. Thus, geometrical deviations can be characterised as a set of unknown time and system dependent functions. In previous attempts, a drift-based deviation model was proposed to integrate a cumulated set of deviations into the aRTist simulation [15]. Even though the proposed model was able to reconstruct the task specific uncertainties of a reference measurement, the approach needed adjusted uncertainty intervals, which had to be provided by an experienced system operator. To resolve this dependence issue, a new approach should only profit from an initial guess of the operator, but otherwise needs to run independently and systematically.

Therefore, several issues have to be solved, like the unknown characteristics of the influencing distributions, the complexity to integrate deviations due to 21 degrees of

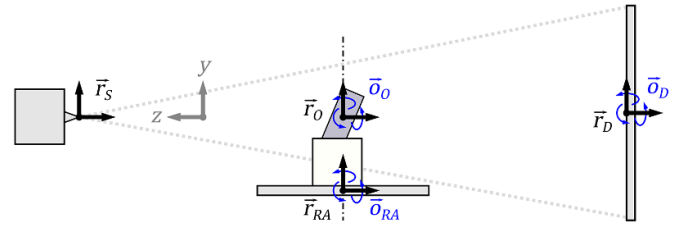


Figure 5. Available parameters in the aRTist *GeoDev* module to add geometrical deviations for each projection during an XCT scan.

freedom (DoF) within the used simulation and the issue of controllability which is necessary to enable automation. Starting with the complexity issue, there are seven parameters in all three dimensions available in the aRTist *GeoDev* module to add geometrical deviations for each projection during a XCT scan. The parameters are visualized in figure 5 and namely: \vec{r}_S position of the source, \vec{r}_O position of the object, \vec{o}_O orientation of the object, \vec{r}_{RA} position of the rotation axis, \vec{o}_{RA} orientation of the rotation axis, \vec{r}_D position of the detector and \vec{o}_D orientation of the detector.

Presuming that there is no prior knowledge about the geometrical deviation distributions during an XCT scan, only the combined interactions of those unknown deviations can be observed in the resulting projection images. However, within this limited view some of the parameters cannot be distinguished anymore. For example, a distortion of the projected image could either be created by a rotation of the object or the detector. A change in scale of the projected image could either be created by a change of the object position or a change of the source and the detector position. Consequently, if only the response characteristic of the unknown deviations is regarded, there exists a set of less than 21 total parameters to describe it.

To identify such a reduced set of parameters, a Pareto analysis (two level variation, 1/8 fraction design) has been conducted with 16 variations of all seven potential parameter groups. Therefore, a common value has been defined which started to create visible artefacts if evenly distributed to all 21 parameters divided equally along the positive coordinate directions. This value was used as the upper limit for the parameter variation, whereas 10% of this upper bound (UB) was set to be the lower bound (LB) for each parameter. As response, the 95% value of the cumulated surface deviations from the nominal to actual surface comparison between the resulting volume and the baseline simulation has been used. Interactions have been iteratively discarded from the analysis, since none crossed the standardized effect line. The resulting Pareto chart of the analysis is displayed in figure 6 and includes four additional variations of the rotation axis position and orientation with levels of 30% and 70% for refinement.

From the chart—which is specific to the chosen geometry setup—can be derived, that an additional variation of the rotation axis orientation during a simulated XCT scan has the most effect on the defined response. The second most important effect was found to be caused by a variation of the rotation axis position, even though it was anticipated that the effects would split into the two blocks orientation or position due to

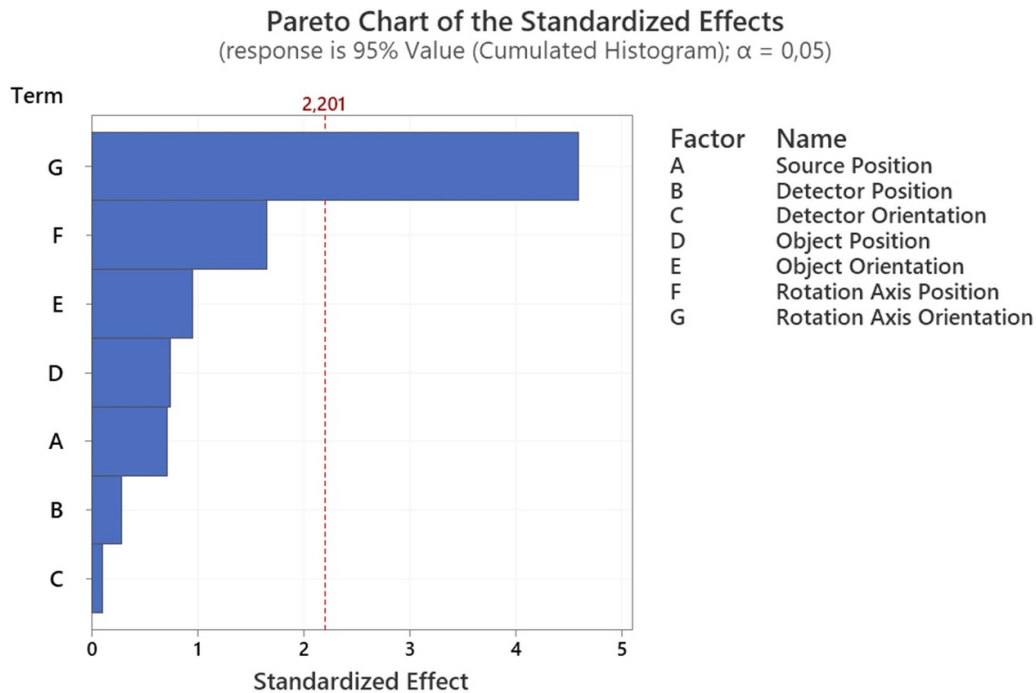


Figure 6. Resulting Pareto chart of the parameter variation study.

their different sensitivity. However, considering that a change of the rotation axis position would also affect the position of the actual measured object—including an additional leverage due to the offset between those coordinate systems—the resulting order can be explained. Since the rotation axis will affect the measured object if either the position or the orientation is changed, the rotation axis can also affect the relative distances or orientations between the object and either the source or the detector. Therefore, to describe the characteristic response of geometric deviations, a reduced set of parameters consisting of \vec{r}_{RA} and \vec{o}_{RA} is further investigated. Regarding the unknown distributions of \vec{r}_{RA} and \vec{o}_{RA} , a Gaussian distribution is chosen as approximation.

3.4. Geometric parameter adaption

In the following sections, two experimental methods will be described regarding the issue of how to integrate geometrical deviations into a simulation model with different XCT systems. Section 3.4.1 will take the baseline simulation described in section 3.1 and use an iterative adaption process to estimate the mean values of the reduced parameter set of section 3.3. Since this approach does not assume any prior knowledge of the target system's geometrical deviations, the method can be characterized as a top-down adaption process. In section 3.4.2, also a reduced set of parameters is used but adjusted to fit radiographically measured positions and orientations of a known geometry. The system and the setup are further described in section 3.4.2.

3.4.1. Iteratively estimated. To systematically reduce a defined comparison parameter between a baseline simulation and a series of measurement references, an iterative adaption

process has been approached. As target reference, a series of 20 repeated measurements of the previously described aluminium hole plate (section 3.1) has been carried out. The measurements were done consecutively, without re-inserting the measurement object or opening the XCT chamber in-between, in order to reduce the influence of the operator, different positioning or thermal conditions. According to section 3.2, the comparison parameter is acquired as follows:

- Determination of the cumulated surface deviation histogram between each single measurement reference and the CMM corrected TSM only for the inner hole ROIs.
- Calculation of the mean cumulated surface deviation graph for the series of measurement references.
- Determination of the cumulated surface deviation histogram of the simulation with the same CMM corrected TSM for the inner hole ROIs.
- Calculation of the squared distance between the cumulated surface deviation graph of the current simulation and the mean graph of the measurement reference series.

The resulting cumulated squared distance (CSD) will be zero, if the cumulated deviations histograms of the simulation and the mean measurement reference are identical and will be greater than zero if divergent. Since the sensitivity of \vec{r}_{RA} and \vec{o}_{RA} are unknown, a single parameter variation for each coordinate has been simulated. The resulting graphs are displayed in figure 7.

Based on the graphs, three observations were made. First, the sensitivity of $r_{RA,y}$ and $o_{RA,y}$ were so low, that they have been excluded from the graphs and will further be neglected. In section 5 this step will be discussed further. Second, all remaining numerical parameters had individual non-linear

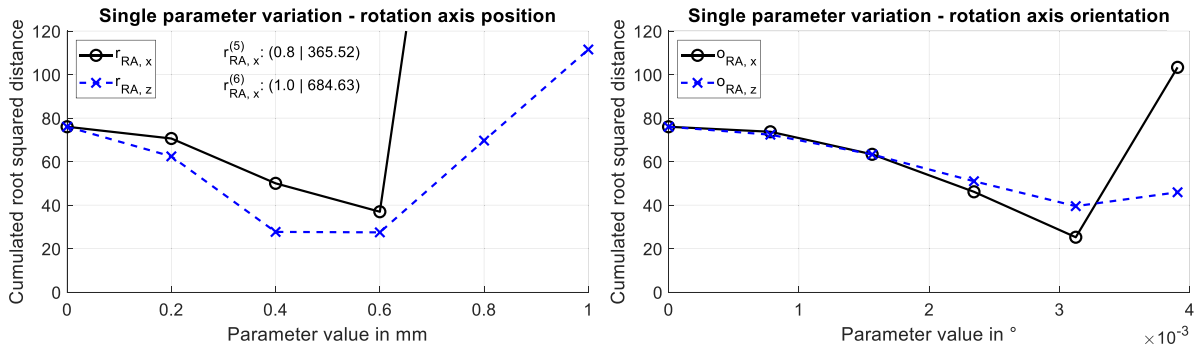


Figure 7. Single parameter variation results for the rotation axis position and orientation.

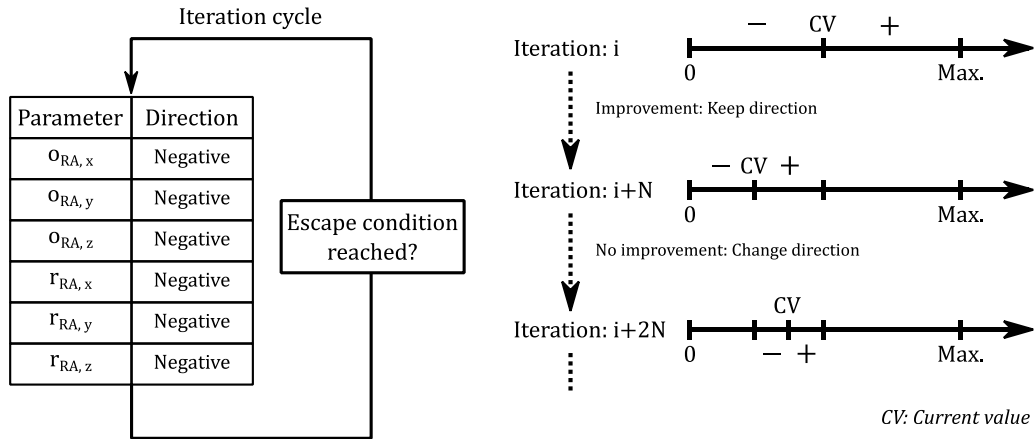


Figure 8. Summary of the used iterative adaption process.

progressions including a local minimum. Last, numerical changes to the rotation axis orientation are more sensitive than changes to the position, which could be expected based on the Pareto study from section 3.3.

Since the CSD is influenced by all remaining parameters, the single parameter variation values cannot be used for the parameter adaption. Furthermore, for a programmatical implementation, there are two additional issues. Currently it is only known, that if no geometrical deviations are added to the simulation, the simulation underestimates the overall deviations compared to the measurement reference (figure 4). Furthermore, every iteration is computationally heavy. For every new CSD the whole measurement process including simulation, reconstruction, surface determination and evaluation has to be completed. Therefore, a progressive parameter adaption process has been implemented, which focusses on reducing the necessary iteration steps for the CSD minimization. The used iterative parameter adaption process is summarized in figure 8.

First of all, a list of N parameters is set up, which includes \vec{r}_{RA} and \vec{o}_{RA} along their coordinate system directions. For every parameter the LB is known to be zero, since if no geometrical deviations are included, the simulation underestimates the measurement reference. The maximum for each parameter is determined based on a single parameter variation. The maximum for each parameter is found, if artefacts or distortions are visible in the resulting volumes, which are known

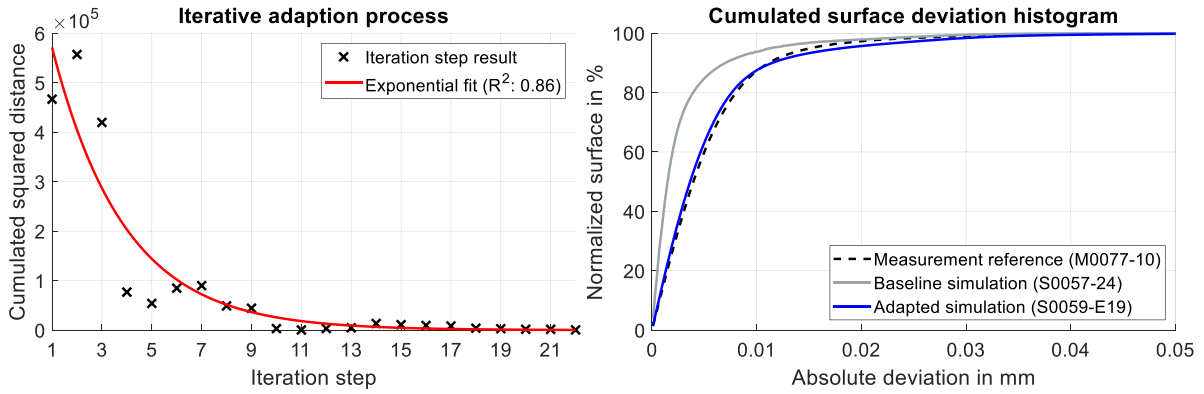
to be not present in the target measurement reference. Then a first iteration is conducted with all parameter maxima used as initial guess. The resulting CSD may be worse than the determined CSDs of the single parameter variation due to the unknown interaction between those. Since the iteration starts with a close to worst case scenario, the directions to change the parameters are known to be negative for initialization. For a fast convergence of the parameters, every new parameter guess is set to be the centre of the interval, which is determined by its current direction. The direction will be flipped, based on the comparison between the resulting CSD value of the current iteration i and the previous iteration. If $CSD_i \leq CSD_{i-1}$ then the current direction of the parameter will be kept and the UB will be set to the current parameter value (CV). If $CSD_i > CSD_{i-1}$ the current direction will be changed to the opposite direction and the LB is set to the CV. In that way, the next CV can be calculated by:

$$CV = LB + \frac{UB - LB}{2}. \tag{1}$$

Thus, the search distance of each parameter is reduced by half with every new guess of the parameter. However, since the direction depends on the previously changed parameter, an interaction between all parameters is integrated. As escape condition to stop the iterative loop, either a defined tolerance can be used or a set of fixed iterations.

Table 2. Initial and resulting parameters (rounded to four decimals) of the adaption process.

Iteration i	$o_{RA,x}$	$o_{RA,z}$	$r_{RA,x}$	$r_{RA,z}$	CSD
1	0.0060°	0.0070°	0.1000 mm	0.1500 mm	466 704
2	0.0030°	0.0070°	0.1000 mm	0.1500 mm	557 018
3	0.0030°	0.0035°	0.1000 mm	0.1500 mm	419 668
...
22	0.0021°	0.0033°	0.0219 mm	0.0329 mm	460

**Figure 9.** Progression of the CSD during the iterative adaption process (left) and the resulting cumulated surface deviation histogram (right).

In case of the previously described simulation, a set of 22 iterations of four sensitive parameters have been evaluated. The first parameter guesses and the resulting parameters are summarized in table 2 and visualized in figure 9.

The progression in-between each iteration (figure 9, left) can be fitted with an exponential function in good agreement and decreases rapidly within the first loop over all considered parameters. The resulting cumulated surface deviation of the iteratively estimated parameters converge to the target graph of the reference measurement (figure 9, right).

3.4.2. Measured. Another possibility to estimate model parameters is to characterise the XCT geometry at operating parameters comparable to those of the XCT scans under investigation. Radiographic analysis of calibrated standards to determine XCT geometry is well established [25]. Here, XCT geometry deviations were determined radiographically using a small, calibrated multi-sphere standard (Zeiss METROTOM-check nano) on a metrology XCT system [26]. Twenty XCT geometries were evaluated from 36 radiographs each according to the method described in [27] over a typical XCT scan time of about 2 h. From the analysis, 9 DoF for the XCT geometry (3 DoF for the x-ray source and 6 DoF for the rotary stage) and 6 DoF for the sample position and orientation on the rotary stage were obtained. Because the method is less sensitive to the rotary axis angular position ($o_{RA,y}$), it was assumed to correspond to the nominal values. This is a valid assumption, since autocollimator measurements on this specific XCT system showed its accuracy to be within $\pm 5 \mu\text{rad}$ [27]. Further, the sensitivity to the absolute values of the source-rotary axis and source-detector distance is reduced depending on the

Table 3. Mean and standard deviation σ of 20 radiographically measured positions and orientations of the rotary axis (\vec{r}_{RA} and \vec{o}_{RA}) and the object (\vec{r}_O and \vec{o}_O). $r_{O,y}$ is held constant because it is directly correlated to $r_{RA,y}$. Coordinate system according to figure 5.

Parameter	Mean	σ
$r_{RA,x}$ (horizontal)	0.019 mm	0.18 μm
$r_{RA,y}$ (vertical)	0.012 mm	0.34 μm
$r_{RA,z}$ (beam axis)	14.115 mm	0.22 μm
$o_{RA,x}$ (pitch)	0.0005°	6.7 μrad
$o_{RA,y}$ ^a (scan angle)	0°	2.9 μrad
$o_{RA,z}$ (roll)	0.0047°	7.9 μrad
$r_{O,x}$	-0.381 mm	0.02 μm
$r_{O,y}$	0.725 mm	—
$r_{O,z}$	0.194 mm	0.01 μm
$o_{O,x}$	-0.27°	5.2 μrad
$o_{O,y}$	339.98°	8.9 μrad
$o_{O,z}$	-0.29°	5.8 μrad

^a Because radiographic sensitivity to $o_{RA,y}$ is low, σ was derived from angular positioning measurements with an optical polygon and an autocollimator [27].

cone-beam angle, whereas magnification can be determined with a high sensitivity below 10^{-5} [27]. Therefore, the source-rotary axis distance ($r_{RA,z}$) was determined for each of the 20 measurements according to $r_{RA,z,i} = \overline{\text{SDD}}/M_i$, where $\overline{\text{SDD}}$ is the mean value of all 20 measurements and M_i the individual magnification of measurement i . As shown in section 3.3, a reduced parameter set can be used to sufficiently parametrize the XCT model. Therefore, the relative offsets between the x-ray source and rotary axis were determined, resulting in 6 relative DoF for the rotary stage. Table 3 shows the mean and standard deviation of the 20 radiographic XCT

Table 4. Input CT geometry parameters for 20 Monte-Carlo iterations derived from stability measurements (static deviation and per angle) and from simulations to estimate the radiographic calibration uncertainty. The values are provided in the coordinate system used in the aRTist module *AdvanCT*.

	Description	Static deviation	σ per scan	σ per angle
X	Horizontal	18.6 μm	2.0 μm	0.5 μm
Y	Beam axis	0.00 μm	0.5 μm	0.5 μm
Z	Vertical	11.8 μm	4.0 μm	0.5 μm
Angle	Rotation around axis	0.0 μrad	0.0 μrad	2.9 μrad
theta θ	Polar angle of axis	87.7 μrad	69.8 μrad	8.7 μrad
phi φ	Azimuthal angle of axis	186.2°	37.0°	26.0°

geometry measurements. The mean values of the object position and orientation describe the alignment of the object coordinate system relative to the rotary table. The standard deviation of the object position was about an order of magnitude smaller than the one of the XCT geometry and thus neglected in the simulations.

The uncertainty of the geometry parameters determined using the radiographic method was assessed with simulations of a multi-sphere standard in aRTist 2 with a known XCT geometry (ground truth) [17], analogous to the method described in [28]. Therefore, 36 projections were simulated and analysed using the same method as for the measured radiographs [27]. From the variance and bias to the ground truth of the thus determined geometry parameters, an uncertainty was estimated and added to the static misalignment parameters prior to each simulated scan iteration (table 4, per scan). From the above measured geometry data (table 3) the XCT geometry was parametrized by static misalignments and probability distributions to describe the non-static behaviour (per angle) and transformed into the aRTist *AdvanCT* module coordinate system (table 4). The standard deviation of the translations was increased to 0.5 μm to account for focal spot drifts [29].

In addition to the geometry deviations, the measured finite x-ray source size, the x-ray spectrum and variations in target current were also included in the simulations. Therefore, the focal spot distribution was measured according to [30] and modelled with five randomly distributed source points weighted by a Gauss–Lorentz distribution (ratio = 0.5) and a FWHM of 2 μm . The spectrum was numerically calculated in aRTist with 80 kV acceleration voltage and a 0.03 mm aluminium filter. The target current was drawn from a uniform distribution with the bounds [62.2 μA , 62.6 μA], which is similar to measured variations. A detector model was created using the *DetectorCalc* module in aRTist with an unnormalized signal-to-noise ratio of 210 measured in a reference flat field and a basic spatial resolution (SR_b) of 0.105 mm from duplex wire measurements.

4. Verification

In the previous chapter, two approaches have been described to either iteratively estimate or measure geometrical deviations and include them into a simulation of a previously generated model. The iteratively estimated approach from section 3.4.1 used the squared distance of the cumulated

Table 5. Imaging parameters for XCT measurement of the hole plate.

Tube voltage	Tube power	Pre-filter	Voxel size	Projections
200 kV	5 W	1 mm Cu	40.066 μm	2000

surface deviations as an optimization criterion to estimate fitting offsets for the position and the orientation of the rotary axis only. To verify the transferability of the general methodology, the approach has been applied in 4.1 to another XCT system (NIKON MCT), but with the same kind of reference sample (aluminium hole plate). Furthermore, 35 unidirectional dimensional features of the baseline simulation and the adapted simulation from section 3.4.1 are evaluated to verify whether the assumption holds, that the minimized surface deviations between the measurement target and the adjusted simulation will also decrease the difference between the same dimensional features. In 4.2 the determined static and dynamic deviations from section 3.4.2 are used to conduct a Monte-Carlo simulation of an MPO fibre ferrule. The resulting dimensional feature deviations are compared to tactile $\mu\text{-coordinate}$ measurement machine (μCMM) reference measurements and used to calculate a task specific measurement uncertainty.

4.1. Transferability and feature deviations

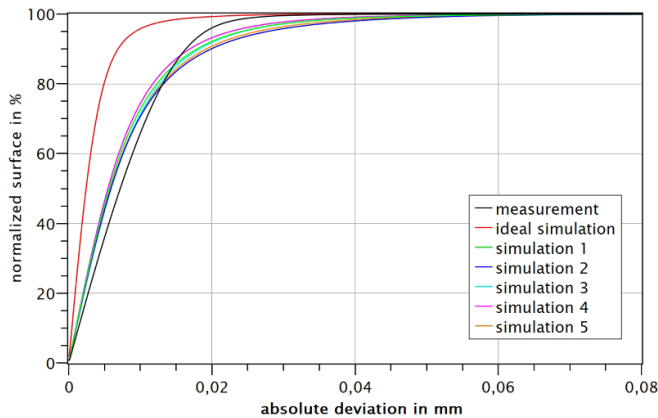
A reference measurement of an aluminium hole plate (PTB_A11) was carried out on a NIKON MCT system with the imaging parameters listed in table 5. The voxel size was determined by a scale calibration using an Invar foil as developed in Activity A1.1.1 of the *AdvanCT* project [5].

The measurement was then represented as a simulation in aRTist using the nominal geometry parameters. The detector model was adjusted to closely match the noise and unsharpness of the measured radiographs and for the detector sensitivity a 600 μm CsI scintillator was assumed. The focal spot was defined as a single point in the simulation to reduce computation time. This simplification was considered feasible because the size of the focal spot at the given x-ray tube settings is estimated to be about 5 μm which is considerably smaller than the voxel size, thus its contribution to the image unsharpness is considered negligible.

Deviations from the nominal geometry were implemented with aRTist's *GeoDev* module and controlled by a MATLAB

Table 6. Initial parameters for geometric deviations.

Parameter	Mean	σ
$r_{RA,x}$ (horizontal)	0.003 mm	0.001 mm
$r_{RA,y}$ (vertical)	0.003 mm	0.001 mm
$r_{RA,z}$ (beam axis)	0.001 mm	0.001 mm
$\phi_{RA,x}$ (pitch)	0.003°	0.001°
$\phi_{RA,y}$ (scan angle)	0.003°	0.001°
$\phi_{RA,z}$ (roll)	0.003°	0.001°

**Figure 10.** Cumulated histograms of the surface deviation between CAD and respective measurement/simulation considering only the surface of the holes.

script, which was also used in section 3.4.1. For the optimization the reduced set of parameters from section 3.3 was used, considering only position and orientation of the rotary axis. The initial parameters were chosen based on measured inaccuracies of the mechanical components of the CT machine as well as previous simulation results. There is a good agreement between measured and simulated results (see table 6).

Using the parameters from table 6 five repeated simulations have been conducted using the cumulated surface distance from section 3.2 as a comparison criterion but with manually adjusted parameters. The resulting cumulated histograms of the surface deviations comparing the measurement data to a simulation with ideal geometry (no geometric deviations) and the simulations with geometric deviations included are illustrated in figure 10.

Without considering geometrical deviations, there is a sharp difference between the cumulated histograms of the reference measurement and the ideal simulation. Analogous to figure 9, the ideal simulation significantly underestimates the surface deviation with a squared distance between the cumulated histograms of 9.8388×10^4 .

Considering only the reduced set of parameters for geometric deviations the simulation results were improved to match the measurement data. The squared distance between the cumulated histograms was reduced to 5.832×10^3 which corresponds to a reduction by 94%, relatively speaking. Comparing the deviations of the nominal/actual comparison locally shows similar distributions for the adapted simulation and measurement reference. The largest deviations of about 30 μm

occur in both cases at the holes close to the edge of the hole plate indicating a slight oval shape of the holes. While the maximal deviations appear to be larger in the simulation their general appearance is similar to those observed in the measurement. Thus, the deformations are not attributed to local geometric deviations, as illustrated in figure 11.

In section 3.2 the surface area of the inner holes of the CMM corrected measurement object CAD was chosen as a suitable evaluation parameter, since typical uni- or bi-directional features can be biased. However, by choosing a surface area as a target value for an optimization it needs to be assessed how the resulting surface deviations influence dimensional measurements. Regarding figure 9, the trend of the cumulated surface deviations of the target measurement and the adapted simulation are similar. Therefore, the total deviations of both surface areas are considered close as well. Although, the cumulated surface histogram does not include spatial distributions. Geometrical features on the other hand, are based on the fit points provided by the local surface they are attached to. To highlight this issue, the centre-to-centre distances of fitted circles centres in the midplane of the hole plate have been evaluated according to [16]. The resulting relative feature deviations compared to the CAD model of the baseline simulation, the adapted simulation and the used target measurement for the adaption process are summarized in figure 12.

The comparison of the uni-directional distances of the target measurement or the simulations show, that even though the cumulated surface deviations of the adapted simulation and the target measurement are similar, there are significant differences ($>10\%$ of the voxel size [31]) considering the resulting features. For example, the worst observed feature deviation (*uni_A2_o26-019*: centre-to-centre distance of hole 26 and 19 along direction A2 see figure 3) differs between the adapted simulation and the measured target reference for 27.9 μm at a voxel size of 39.9 μm . Considering directions, most of the total differences stack along the A1 and the A2 direction (see figure 3), which indicates that there is a directional dependency in the adapted simulation, which has not been there either in the target measurement or the baseline simulation.

4.2. Monte-Carlo uncertainty estimation with measured XCT deviations

To verify if the model parameters enable us to estimate appropriate measurement uncertainties, an MPO fibre ferrule with two guide pin holes (\varnothing 0.699 mm) and 24 fibre holes (\varnothing 0.126 mm) made of a high-performance thermoplastic was used as a reference object (figure 13). It was XCT scanned on a metrology XCT system [26] by recording 3000 projections on a circular trajectory with a total scan time of about 3.5 h. The x-ray source was operated at 80 kV with a set target current of 63 μA . Data were reconstructed with a voxel size of 2 μm in CERA 5 (Siemens) after the horizontal rotary axis offset was corrected from projection data. Volume data were analysed in VG Studio MAX 3 (Volume Graphics) as follows: Advanced surface determination based on grey value gradient, registration of the object, data evaluation by

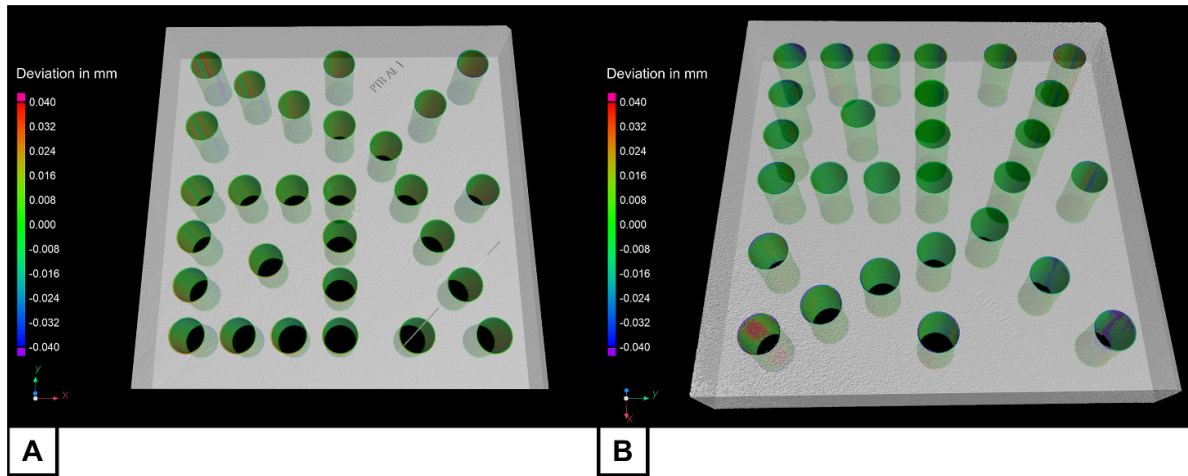


Figure 11. Visualization of the nominal/actual comparison for measurement (A) and simulation with geometric deviations after five iterations (B).

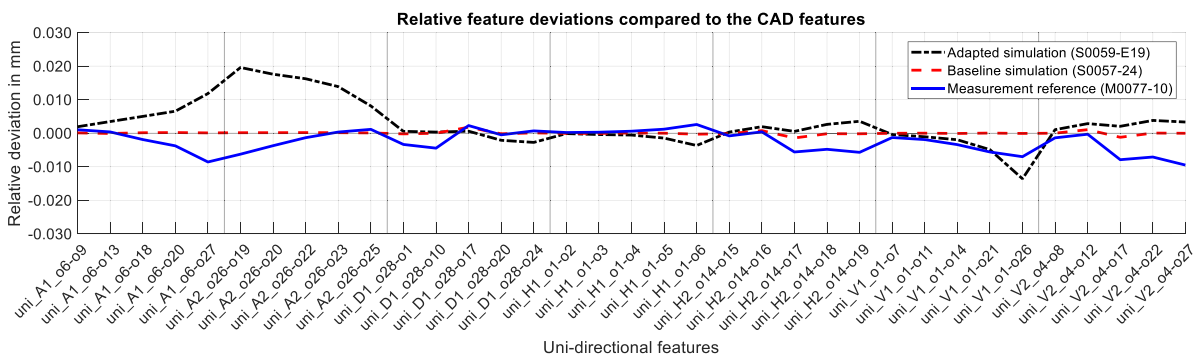


Figure 12. Relative feature deviations of the adapted simulation, the baseline simulation (compare figure 9) and the target measurement reference compared to the CAD features.

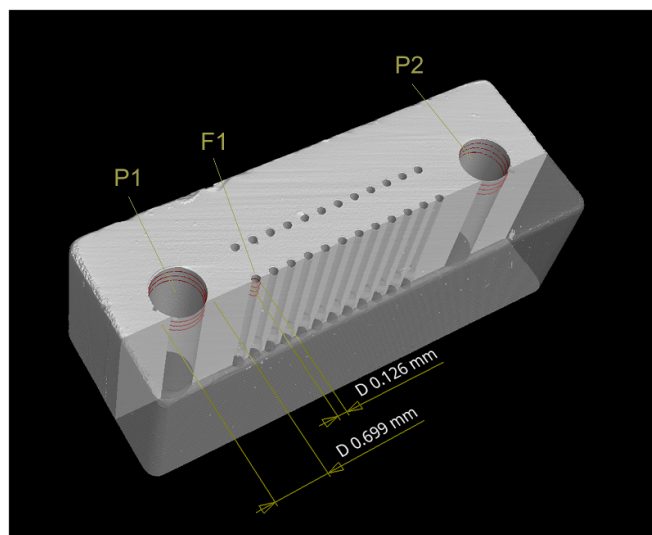


Figure 13. Rendering of the measured XCT data of the MPO fibre ferrule, consisting of two guide pin holes (P) and 24 fibre holes (F). Tactile reference data was measured for the guide pin holes P1 and P2 at three measurement heights indicated by the red circles (−0.1 mm, −0.2 mm and −0.3 mm from the surface).

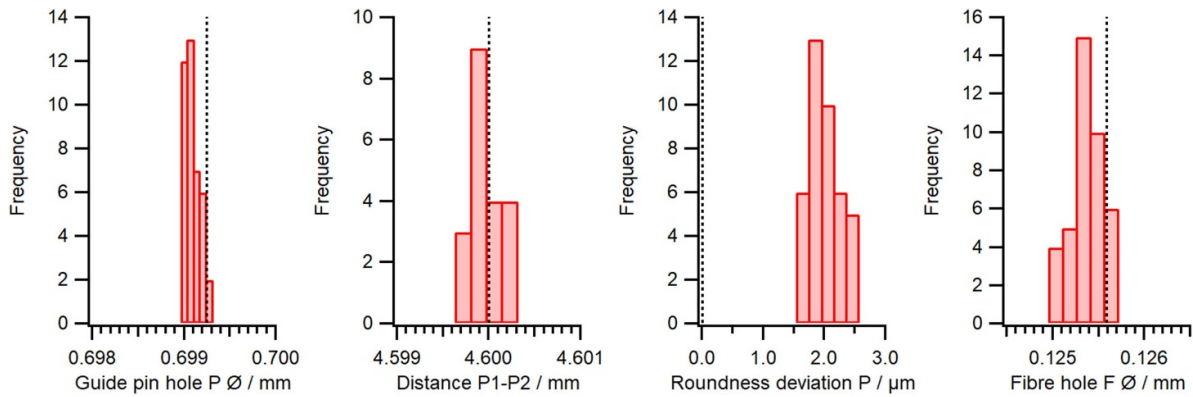


Figure 14. Distributions derived from 20 Monte-Carlo simulations for the guide pin hole (P Ø) and fibre hole (F Ø) diameters, the guide pin hole distance (P1–P2) and their roundness deviation. The dashed line represents the reference values measured on the STL file used as an input for the simulations.

Table 7. Measurement uncertainty estimated from the Monte-Carlo simulations for different features (figure 14).

Feature	Diameter guide pin hole P	Distance guide pin holes L	RONt guide pin hole P	Diameter fibre hole F
Standard deviation σ	0.09 μm	0.19 μm	0.26 μm	0.17 μm
Bias b	-0.18 μm	-0.04 μm	1.98 μm	-0.23 μm
$U_{k=2} = 2\sqrt{\sigma^2 + b^2}$	0.4 μm	0.4 μm	4.0 μm	0.6 μm

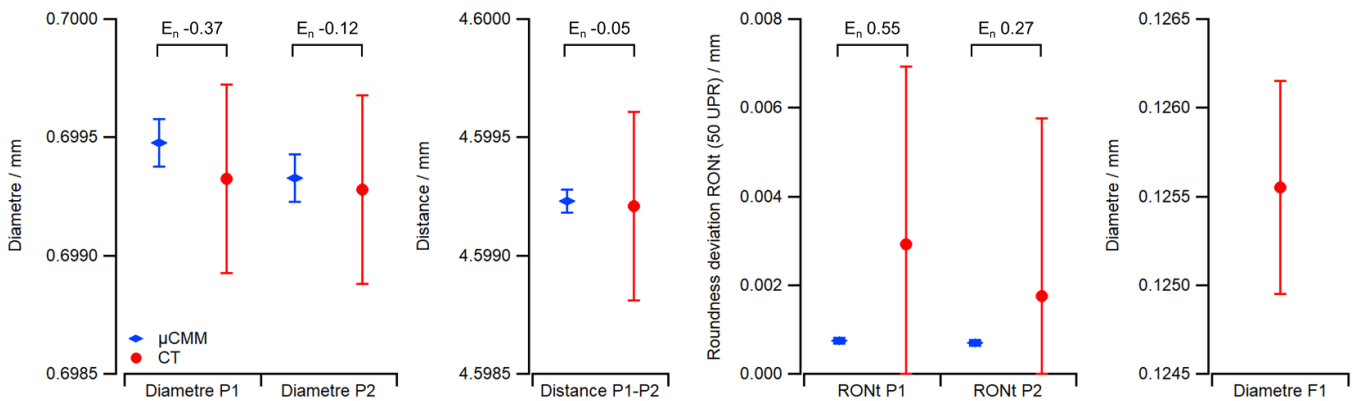


Figure 15. Comparison between tactile μCMM and XCT measurements. Three different measurement positions (see figure 13) were averaged. The agreement between the measurements was evaluated using the normalised error E_n . The fibre holes could not be probed on the tactile μCMM .

fitting circular primitives in the same positions as the reference calibration data. Reference calibrations were performed on a tactile μCMM using a 125 μm ruby sphere in scanning mode [32]. The two guide pin holes were probed at three heights as indicated by the red circles in figure 13.

Geometry deviations from table 4 were used as an input for 20 iterations of the XCT measurement simulated in aRTist 2 [17]. A stereolithographic file (STL) generated from the CAD model of an optical fibre ferrule, similar to the one in figure 13, was used in the simulations. Data from simulations were reconstructed and analysed in exactly the same way as the measurement data. Figure 14 shows the resulting distributions and the reference values from the STL file. In table 7, the task specific measurement uncertainties were estimated according to [15]. Whereas sub-micrometre uncertainties were

calculated for diameter and length measurements, the uncertainty of the roundness deviation was several micrometres. This is attributed to the fact that roundness is a peak-to-peak measure and, thus, more prone to noise in the volume data.

To assess the validity of the measurement uncertainty estimation, XCT data was compared to tactile μCMM data in figure 15. All measurements agreed within their measurement uncertainties ($E_n < 1$), proving that sub-micrometre uncertainties can be achieved even for bidirectional diameter measurements that rely on the surface determination. To achieve such low uncertainties, a highly accurate XCT system [26] in combination with a small sample, resulting in small voxels, are a prerequisite. Furthermore, high surface quality, low form errors and a material that causes little artefacts, i.e. with a low absorption coefficient, are essential.

5. Discussion

In the previous chapters some challenges towards a general methodology to determine geometrical deviation model parameters have already been highlighted. First, geometrical deviations cannot be neglected in the surveyed XCT systems. The cumulated surface deviations of the baseline simulation from the Metrotom (figure 9) and the Nikon (figure 10) systems both underestimated the surface deviations of reference measurements, which indicates a general underestimation of error sources in the simulation. Due to the variety of the sources causing geometrical deviations in XCT (e.g. temperatures, vibrations, misalignments) several simplifications or assumptions had to be made, like the fixation of a processing framework (section 3.1).

The suggested framework may reduce the influence of different algorithmic implementations (e.g. reconstruction, surface determination), but it will not always be beneficial. For example, if only the projections are taken as common interface between simulation and measurement, some system specific correction methods cannot be applied anymore. For example, in case of the Metrotom system, a geometrical correction method is integrated in the reconstruction process, which either requires to use the manufacturers reconstruction software or lose that information in the process. In case of the Metrotom adaption, the FDK reconstruction from VG Studio MAX (v. 3.5) has been used for the simulation and the measurement reference, which may partially explain some of the resulting feature differences of the target measurement towards the CMM corrected CAD features in figure 12.

Another issue may be the imperfection of the baseline simulation itself. For example, in the described Metrotom baseline adaption, no dynamical deviations are considered (e.g. variation of the x-ray source current or acceleration voltage during the scan). Consequently, the iterative estimated parameters from section 3.4.1 mapped those unhandled error sources as geometrical deviations. In case of the presented adaption, dynamical deviations have not been focused on, since the static CSD offset of the 20 reference measurements towards the baseline simulation was dominant compared to the maximum range of the repeated measurements CSDs.

An unexpected result of the iterative parameter estimation (section 3.4.1) was demonstrated in figure 12. Despite the cumulated surface deviation curve of the adapted simulation and the target measurement being similar in shape and with a small CSD, the extracted features of the resulting surfaces still deviate significantly in some cases prohibiting a useful application of the iterative methods in its current state. As described in section 4.1, the stacked deviations along the directions A1 and A2 indicate a directional dependency, which has been introduced by the adaption process since the baseline simulation does not show the same behaviour. A possible explanation may be the missing sensitivity of $r_{RA, y}$ and $o_{RA, y}$, which was observed in the single parameter variation for figure 7. Regarding the parameter definitions of the used *GeoDev* module in figure 5, a conjunction of the rotation axis and the measurement object is expected as it is in an actual XCT system. However, simulated geometrical deviations along the rotation

axis y -direction had no influence on the resulting CSD, which is the reason the parameters have been excluded from the iterative adaption routine in table 2. Without a sensitivity along the y -direction, there are only 4 DoF left for the optimization process. Consequently, any necessary changes along the y -axis are mapped on the z - and x -axis parameters, which probably contributed to the observed directional dependency. Due to this issue, a further extension of the iterative method towards a task specific uncertainty was not reasonable.

Furthermore, in prior approaches to manually adjust the geometrical deviation parameters, local surface deviation hotspots were observed, despite well-matching cumulated surface deviation shapes and a small CSD [25]. Such obvious local deviation hotspots have not been observed using the automated iterative adaption process in section 3.4.1. However, the presented parameter search algorithm was designed to converge fast, due to the high computational time investment for each iteration. Reducing the step size by half for every whenever a parameter is evaluated, the fast convergence behaviour comes with drawbacks. The minimal CSD value for the 22 iterations was already reached in iteration 11 (compare figure 9). Also, a constant reduction of the step size does also not address local minima during the adaption process. A standardized multi-objective optimization may handle those issues better. Besides, high performance computing solutions for XCT simulations are becoming more popular, which provides a solid infrastructure to handle the computational overhead of iterative methods. However, regarding controllability and the observed convergence behaviour of the iterative parameter adaption routine (section 3.4.1), the presented method is still promising towards a fully automated parametrization process. Though, the issue with the directional dependencies has to be resolved first. A potential improvement may be, to use the local surface deviations of each hole separately instead of the cumulated surface deviations as input for the optimization.

As a complementary approach to the iterative geometry optimization, a direct radiographic measurement of the XCT geometry deviations was investigated. It is based on repetitive measurements of a calibrated multi-sphere standard to determine the XCT geometry and its variability. Since radiographic geometry measurements should be performed at similar operating conditions to the actual XCT scan to ensure a comparable drift behaviour, it is experimentally elaborate. However, besides determination of model parameters, it enables identification and possible compensation of geometric error sources. Applying the approach on a research metrology XCT system, resulted in task specific expanded measurement uncertainties below one micrometre for bi-directional features.

6. Conclusion

In this work, an insight into the methodologies to determine parameters for virtual XCTs has been given. Therefore, a framework suggestion to integrate virtual models into the XCT measurement process has been described. The framework takes any kind of combination of XCT system and radiographic simulation software focussing on similar conditions

in the dimensional XCT processing chain. In the follow-up section 3.2, a suitable quantity to compare simulated volumes and measured volumes is briefly discussed. The CSD of the resulting surface deviations histograms compared to a CMM corrected TSM model is used as a parameter to quantitatively describe the similarity between those graphs by a single value. Since geometrical deviations are considered to be a missing key element to represent XCT systems in simulations, two experimental methods are described to integrate them into an aRTist simulation. In section 3.4.1 an experimental approach is presented to iteratively estimate a reduced set of geometrical deviation parameters by minimizing the CSD. The second approach from section 3.4.2 determines a reduced set of geometrical deviation parameters based on radiographically measured distributions. Both approaches have been individually verified, either by transferring them to other XCT systems or measured objects. The radiographically measured approach was found to be in good agreement even for bi-directional task specific feature uncertainties. Whereas the iteratively estimated approach revealed some unhandled directional dependencies and requires further improvement.

In conclusion, computed tomography is a fast-growing sector for industrial applications. However, without a traceable and time efficient method to determine the uncertainties for a measurement, the possible applications are limited. With a digital twin of an XCT system, this limit may be overcome but it requires a closely adapted model of the actual XCT system. Within this work, two systematic methods to integrate geometrical deviations to a simulation model have been presented and discussed. Which is a necessary step forward towards the development of a true digital XCT twin [33].

Data availability statement

The data that support the findings of this study are available upon reasonable request from the authors.

Acknowledgments

This work is part of the European Metrology Programme for Innovation and Research (EMPIR) project 17IND08 AdvanCT. The EMPIR initiative is co-funded by the European Union's Horizon 2020 research and innovation programme and the EMPIR participating states.


Authors contribution

Felix Binder (F B) contributed to conceptualization and validation. Data curation, formal analysis, visualization and writing of the original draft was done by Benjamin A Bircher (B B), René Laquai (R L) and F B. Felix Meli (F M), Carsten Bellon (C B), F B and B B contributed to methodology and software. Alain Küng (A K), F B, B B and R L contributed to the investigation process. Supervision was provided by Tino Hausotte (T H) and F M. Ulrich Neuschaefer-Rube (U N), F M, B B

and T H contributed to funding acquisition and project administration. Andreas Deresch (A D), F B, B B, F M, A K, R L and C B contributed to review and editing.

ORCID iDs

Felix Binder  <https://orcid.org/0000-0003-1781-779X>

Benjamin A Bircher  <https://orcid.org/0000-0002-1494-6732>

Carsten Bellon  <https://orcid.org/0000-0002-3861-8426>

Felix Meli  <https://orcid.org/0000-0001-7575-7540>

Ulrich Neuschaefer-Rube  <https://orcid.org/0000-0002-5122-8799>

Tino Hausotte  <https://orcid.org/0000-0002-2923-3217>

References

- [1] Verein Deutscher Ingenieure e. V 2015 VDI/VDE 2630 Part 2.1—computed tomography in dimensional measurement—determination of the uncertainty of measurement and the test process suitability of coordinate measurement systems with XCT sensors Düsseldorf
- [2] Joint Committee for Guides in Metrology 2008 Evaluation of measurement data—supplement 1 to the “guide to the expression of uncertainty in measurement Propagation of distributions using a Monte Carlo method
- [3] Microparts project website Multi-sensor metrology for microparts in innovative industrial products (available at: www.ptb.de/empir/microparts-home.html) (Accessed 01 October 2021)
- [4] Helmecke E, Fleßner M, Kaufmann M, Staude A and Hausotte T 2016 Numerical measurement uncertainty determination for dimensional measurements of microparts with XCT *6th Conf. on Industrial Computed Tomography* (Wels, Austria)
- [5] AdvanCT project website 17IND08 AdvanCT—advanced computed tomography for dimensional and surface measurements in industry (available at: www.ptb.de/empir2018/advanct/home/) (Accessed 01 October 2021)
- [6] Bellon C and Jaenisch G-R 2007 aRTist—analytical RT inspection simulation tool. *Presented at DIR 2007—Int. Symp. on Digital Industrial Radiology and Computed Tomography* (Lyon, France, 25-27 June 2007) (available at: www.ndt.net/article/dir2007/papers/s1.pdf)
- [7] Bellon C, Deresch A and Jaenisch G-R Radiography simulation with aRTist—combining analytical and Monte Carlo methods *Digital Industrial Radiology and Computed Tomography (DIR 2015) (Belgium)* (available at: www.ndt.net/?id=18074)
- [8] Hiller J, Fuchs T O J, Kasperl S and Reindl L M 2011 Einfluss der Bildqualität röntgentomographischer Abbildungen auf Koordinatenmessungen: Grundlagen, Messungen und Simulationen *Tech. Mess. Tm* **78** 334–47
- [9] Reiter M, Erler M, Kuhn C, Gusenbauer C and Kastner J 2016 SimCT: a simulation tool for x-ray imaging *Presented at 6th Conf. on Industrial Computed Tomography, 2016 (Wels, Austria)* (available at: www.ndt.net/?id=18746)
- [10] Fernandez R, Costin M, Tisseur D, Leveque A and Legoupil S 2012 CIVA computed tomography modeling. *Presented at 18th World Conf. on Nondestructive Testing, 2012 (Durban, South Africa)* (available at: www.ndt.net/?id=12658)
- [11] Reiter M and Kastner J 2016 Investigation towards simulation-based determination of measurement uncertainties for x-ray computed tomography *4th Int. Conf.*

- on Image Formation in X-ray Computer Tomography (Bamberg, Germany)*
- [12] Hiller J and Reindl L M 2012 A computer simulation platform for the estimation of measurement uncertainties in dimensional x-ray computed tomography *Measurement* **45** 2166–82
- [13] NanoXSpot project website 18NRM07 NanoXSpot measurement of the focal spot size of x-ray tubes with spot sizes down to 100 nm (available at: www.ptb.de/empir2019/nanoxspot/home/) (Accessed 01 October 2021)
- [14] CTSimU project website WIPANO—CTSimU (available at: www.ctsimu.forschung.fau.de/) (Accessed 01 October 2021)
- [15] Wohlgemuth F, Müller A M and Hausotte T 2018 Development of a virtual metrological XCT for numerical measurement uncertainty determination using aRTist 2 *Tech. Mess. Tm* **85** 728–37
- [16] Sato O Instruction of hole plate measurement using the supplied templates October 2013. Internal reference
- [17] Bundesanstalt für Materialforschung und –prüfung aRTist—analytical RT inspection simulation tool (available at: www.artist.bam.de/) (Accessed 11 January 2022)
- [18] Binder F, Bellon C, Wohlgemuth F and Hausotte T 2021 Ein praxisnaher Leitfaden für computertomografische Untersuchungen mit der radiografischen Simulationsumgebung aRTist Presented at DGZfP-Jahrestagung 2021 (Germany) (available at: <https://jahrestagung.dgzfp.de/portals/jt2021/bb176/inhalt/p4.pdf>)
- [19] Bellon C, Binder F and Plotzki D *aRTist Handbook* (available at: <https://bamresearch.github.io/aRTist-handbook/>) (Accessed 11 January 2022)
- [20] Orgeldinger C, Wohlgemuth F, Müller A and Hausotte T 2019 Spot size and detector unsharpness determination for numerical measurement uncertainty determination *Proc. 9th Conf. on Industrial Computed Tomography (Padova)* (available at: www.ndt.net/?id=23649)
- [21] ASTM E1165-12 2017 Standard test method for measurement of focal spots of industrial x-ray tubes by pinhole imaging
- [22] ASTM E2597/E2597M-14 Standard practice for manufacturing characterization of digital detector arrays
- [23] DIN EN ISO 15708-3:2019-09 Non-destructive testing—radiation methods for computed tomography—part 3: operation and interpretation (ISO 15708-3:2017)
- [24] Wohlgemuth F, Bellon C and Hausotte T 2020 Measurement-based detector characteristics for digital twins in aRTist *20th World Conf. on Non-Destructive Testing (Korea)* accepted
- [25] Ferrucci M, Leach R K, Giusca C, Carmignato S and Dewulf W 2015 Towards geometrical calibration of x-ray computed tomography systems—a review *Meas. Sci. Technol.* **26** 092003
- [26] Bircher B A, Meli F, Küng A and Thalmann R 2020 METAS-XCT: metrological x-ray computed tomography at sub-micrometre precision euspen's *20th Int. Conf. & Exhibition (Geneva, Switzerland)*
- [27] Bircher B A, Meli F, Küng A and Thalmann R 2019 XCT geometry determination using individual radiographs of calibrated multi-sphere standards *9th Conf. on Industrial Computed Tomography (ICT 2019) (Padova, Italy)*
- [28] Ferrucci M, Heřmánek P, Ametova E, Carmignato S and Dewulf W 2018 Measurement of the x-ray computed tomography instrument geometry by minimization of reprojection errors—implementation on simulated data *Precis. Eng.* **54** 7–20
- [29] Bircher B A, Meli F, Küng A and Thalmann R 2020 X-ray source tracking to compensate focal spot drifts for dimensional XCT measurements *10th Conf. on Industrial Computed Tomography (Wels, Austria)*
- [30] Bircher B A, Meli F, Küng A and Sofienko A 2021 Traceable x-ray focal spot reconstruction by circular edge analysis: from sub-microfocus to mesofocus *Meas. Sci. Technol.* **33** 074005
- [31] Reinhard C 2008 Industrial computer tomography—a universal inspection tool *17th World Conf. on Nondestructive Testing (China)*
- [32] Küng A, Meli F and Thalmann R 2007 Ultraprecision micro-CMM using a low force 3D touch probe *Meas. Sci. Technol.* **18** 319–27
- [33] CASRAI CRediT—contributor roles taxonomy (available at: <https://casrai.org/credit/>) (Accessed 11 January 2022)